# Ion yield enhancement at the organic/inorganic interface in SIMS analysis using Ar-GCIB

V. Cristaudo[a,b,*], C. Poleunis[a], P. Laha[b], P. Eloy[a], T. Hauffman[b], H. Terryn[b], A. Delcorte[a]

[a] *Université Catholique de Louvain, Institute of Condensed Matter and Nanosciences, 1 Place Louis Pasteur Box L4.01.10, B-1348 Louvain-la-Neuve, Belgium*
[b] *Vrije Universiteit Brussel, Research Group Electrochemical and Surface Engineering, Department of Materials and Chemistry, 2 Pleinlaan, B-1050 Brussels, Belgium*

## ARTICLE INFO

## ABSTRACT

Argon gas cluster ion beams (Ar-GCIBs) provide new opportunities for molecular depth profiling and imaging of organic materials and biological samples, thanks to recent technological developments that have led to the construction of new SIMS spectrometers where the traditional issues related to their low lateral resolution along with poor mass resolution and mass accuracy are overcome. The present fundamental contribution on SIMS molecular depth profiling investigates the variations of the secondary ion signals observed at the organic–inorganic hybrid interface when using Ar-GCIB as the analytical beam. With this in mind, depth profiling experiments were performed with a ToF-SIMS spectrometer using different analysis beams: 30-keV $Bi_5^+$ versus 10-keV $Ar_n^+$ with a cluster size ($n$) of 800, 1500, 3000 and 5000 atoms, respectively. A 10-keV $Ar_{3000}^+$ beam was used for sputtering in all the experiments. Irganox 1010 and model polymers such as polystyrene (PS) and poly (methyl methacrylate) (PMMA) oligomers were chosen. Silicon wafer and a polymer-based substrates were employed to test materials with different stiffness, which is directly related to their Young's moduli, an important parameter in this study. Ar-GCIB depth profiles systematically show ion signal enhancement of the characteristic fragments of PS and Irganox 1010 when approaching the interface with the silicon substrate, that can reach up to 60% for $[M_{1010}-H]^-$ in Irganox films deposited onto silicon wafers. This enhancement increases with increasing $n$ in both ion polarities. These results point out some ionization effects on the observed signal enhancement at the interface. The experimental observations will be explained on the basis of the physics of the impact of large argon clusters on different target materials and the energy confinement of the ion projectile in the organic overlayers. Finally, the thickness of organic films on rigid substrates in the nanoscale appears to be a crucial parameter to dramatically improve the sensitivity to molecular fragments when using large Ar cluster ions as analysis beams.

## 1. Introduction

In the past decade, large gas cluster ion beams (GCIBs) using mostly $Ar_{250-10000}^+$ clusters rapidly became very popular in secondary ion mass spectrometry (SIMS) as a universal sputter source for organic and polymer-based materials [1–3], in a large spectrum of applications ranging from electronic devices [4,5] to biological analysis [6]. The great success of these sputter beams, as was explained by simulation studies, is due to the minimal molecular degradation and fragmentation induced by the massive cluster impact (closer to the concept of desorption) compared to that of smaller polyatomic projectiles such as fullerene ions [7,8]. A very recent study introduces the Ar-GCIB-$O_2^+$ cosputtering in order to enhance the ionization yield of soft materials (polymers) and minimize or mask the artifacts in the depth profiles (especially the decay in the ion intensity at the steady state), resulting

from the inevitable (low) alteration of the chemical structure induced by the large Ar clusters [9]. Furthermore, several groups have also reported considerable benefits in the use of the Ar-GCIBs as analysis probe for biological imaging compared to the more traditional bismuth cluster ion beams [10] due to a relative augmentation of the high-mass secondary ion yields. However, in conventional time-of-flight (ToF)-SIMS instrumentation, the application of Ar-GCIBs as analysis beams is limited by the low mass resolution and mass accuracy that prevents the identification of unknown peaks, as well as poor focusing properties and sometimes, low ionization efficiency [10]. In this context, the delayed extraction procedure combined with external mass calibration can help to improve the mass resolution and mass accuracy of the spectrum or image [11,12]. It consists of applying an extracting voltage of the secondary ions with a specific time delay after the primary beam hits the surface, in order to operate time-of-flight compensation on the

ion energy spread. Unfortunately, mass spectra acquired in the delayed extraction mode lose the low mass peaks – namely the hydrogen ion and carbon fragments – which, in addition to asymmetric peaks in the low $m/z$ range, makes the application of internal mass calibration very difficult (the standard procedure in ToF-SIMS) [12]. Recently, instrumental developments have led to the construction of SIMS spectrometers where GCIB sources are operated either in quasi-continuous mode to work in combination with an Orbitrap analyzer (3D OrbiSIMS) [13], or in continuous mode bunching the secondary ion stream obtained with a high energy primary beam (J105 Chemical Imager) [14], to achieve both high mass resolution and high spatial resolution simultaneously. Therefore, we have entered in a golden age of SIMS where the GCIBs start to provide new opportunities for molecular depth profiling and imaging of organic materials and biological samples.

In this context, our contribution aims at clarifying the characteristic features of the depth profiles when using Ar-GCIBs, especially in the interfacial regions. Indeed, organic and organic–inorganic interfaces are of great technological interest in many applications as, for example, in drug delivery systems where the drug phase separates from the polymer matrix in order to accumulate at both the surface and the buried interface. In such systems, it is crucial to understand whether the signal variations when approaching the interface with a given substrate correspond to real modifications in the analyte concentration or whether they are possible artifacts [15]. Matrix effects have been studied in binary mixtures of Irganox 1010 and Irganox 1098 by Shard et al. in the bulk region [16], disregarding both transient changes at the surface mostly related to damage accumulation and increased intensities at the interface, which are very complex to investigate. In the SIMS literature, it has been demonstrated that intensity changes at the interface are not affected by the adventitious alkali contamination of the substrate [17], excluding the possibility of matrix-enhanced SIMS [15,18]. Removal of matrix and roughening effects at both interfaces of FMOC to Irganox 1010 and Irganox 1010 to FMOC has been attempted more recently [19], obtaining consistent compositional profiles for all the ions that are described by an integrated exponentially modified Gaussian profile. Finally, the interface positions in this organic system using SIMS depth profiles with GCIB sputtering and negative secondary ions have been successfully determined.

To achieve the goals of the current study, organic thin films were spin coated onto a harder substrate, silicon. Irganox 1010 was chosen as the reference material because of its fragmentation in the high $m/z$ range, as well as the possibility to detect the molecular ion in both negative and positive ion polarities. Model polymer films of monodisperse polystyrene (PS) were also included in the study, since they allow us to work at low mass resolution in the TOF.SIMS 5 instrumentation with 10-keV $Ar_n^+$ with $800 \leq n \leq 5000$, both in the analysis and sputtering mode. Indeed, as they only contain C and H atoms, mass interferences are limited. The results show that the effect of the silicon substrate on the secondary ion intensities is larger when Ar-GCIBs are used for the analysis instead of the usual analysis beams ($Bi_n^+$). The comparison of different GCIB projectiles indicates that the secondary ion intensities are also affected by the average energy per atom of the primary ions, $E/n$. The possible causes of the observed effects, namely changes in the sputtering, fragmentation and/or ionization near the interface, are investigated in detail.

### 1.1. Strategy and article structure

In this paper, we first assessed the presence of secondary ion yield enhancement at the interface of the Si-supported Irganox 1010 overlayer with large Ar cluster analysis by means of two independent protocols, namely Ar-GCIB depth profiling and static-SIMS with an Ar-GCIB analysis beam on films of increasing thickness. This rise of the secondary ion signals at the interface was suspected to be due to ionization/matrix effects, which was verified by the change of ion polarity. In fact, based on our experience on photovoltaic systems, matrix effects should be more pronounced in one given ion mode because of preferential charge-

transfers. It was found that such effects cannot be ruled out in the case of the Irganox 1010 system. Then, the two other effects that can be identified as main contributions to the secondary ion yield enhancement are fragmentation and sputtering effects. An enhancement of the sputtering yield in the ultrathin scale of a depth profile due to energy nanoconfinement was already the subject of study of our previous publication [20]. This effect was confirmed on Irganox 1010 ultrathin films with new sputtering yield calculations on the system under investigation at two different etching conditions. Therefore, the authors decided to prioritize the novelty of the fragmentation study at the interface of Irganox 1010 films with respect to the order of importance of the different contributions. Here, two additional model polymer systems, namely PS and PMMA, were taken into account to determine whether the phenomenon was sample-dependent or not. A proper methodology was established for the fragmentation study by defining ion signal enhancements at the interface together with ion signal shifts with respect to the silicon substrate in both ion polarities. Finally, it was found that fragmentation determined by energy nanoconfinement is playing an important role in the observed interface phenomenon. However, the main effect in the specific case of Irganox 1010 films is related to sputtering enhancement at the interface as it will be demonstrated at the end of the present work when comparing the three different contributions – ionization, fragmentation and sputtering.

## 2. Experimental methods

### 2.1. Samples

The silicon wafer substrates (Neyco S.A., Vanves, France) covered by a 1.3-nm thick native oxide layer (measured by XPS, Section 2.2) were cleaned by sonication in isopropanol (VWR, HPLC grade, 99.9%) and dried under a nitrogen flux prior to spin coating, in order to eliminate any dicing dust and contaminants. A second series of silicon wafers was cleaned with a piranha solution, a 4:1 mixture of concentrated sulfuric acid and hydrogen peroxide (both provided by VWR BDH Prolabo, Leuven, Belgium), in order to effectively remove the organic contamination from the substrate and also to compare with the isopropanol cleaning. The wafers were then rinsed in deionized water for three cleaning cycles and once with absolute ethanol (VWR, purity 99.8%). Finally, the substrates were dried using nitrogen gas and cleaned with UV/ozone (Jelight Company Inc., Irvine, USA) for a further 10 min.

The reference material, Irganox 1010 ($C_{73}H_{108}O_{12}$, $M_w = 1177.6$ g/mol), also known as pentaerythritol tetrakis(3-(3,5-di-*tert*-butyl-4-hydroxyphenyl)propionate, is a chemical compound composed of four sterically hindered phenols linked through a pentaerythritol core. It is used as primary antioxidant for stabilizing polymers, particularly polyethylene and polypropylene. Irganox 1010 was sourced from Ciba Specialty Chemicals Inc. (Basel, Switzerland). The powder sample was dissolved to reach a concentration of $\sim 20$ mg/mL in toluene (Sigma-Aldrich, $\geq 99.71\%$ purity) and spin coated (acceleration: 20 000 rpm/s, speed: 5000 rpm and time: 60 s) onto clean silicon wafers of $1 \times 1$ cm$^2$ in order to prepare thin films of approximately 50-nm thickness. Toluene is a low-pressure vapor solvent known for providing very smooth surface morphologies upon spin coating [21,22], an important requirement for the measurement of the sputter efficiency and interface studies. Spin coating represents a valid alternative to thermal evaporation [23] in terms of uniformity and flatness of single-layers of Irganox 1010 on silicon substrates.

The Irganox 1010 solution was also spin coated onto polyethylene terephthalate (PET) $\sim 1 \times 1$ cm$^2$ supports of 1-mm thickness. Goodfellow Inc. provided the amorphous PET sheet covered by protective film on both sides. No cleaning procedure was performed prior to spin coating, in order to avoid contamination evidenced by previous SIMS analyses [24]. In addition, a series of thin Irganox 1010 films with 1–50 nm thickness (samples A-F) was prepared by spin coating six different solutions in toluene with concentrations ranging from 0.8 to

21.6 mg/mL onto clean silicon wafers (sonicated in isopropanol). Finally, Irganox 1010 thin films of thickness ranging from 10 to 200 nm were prepared to determine the variation of the sputter yield volume along a depth profile experiment when using two different 10-keV $Ar_n^+$ sputter conditions, i.e. $n = 1500$ and $n = 5000$ (two measurements per sample). Two independent techniques - ellipsometry and profilometry - were employed to measure the film thickness and the sputter crater size, respectively. The sputter yield volumes $Y$ ($nm^3$ per incident ion) were calculated by dividing the total sputtered volume ($nm^3$) by the primary ion dose (ions) needed to reach the interface with the native silicon oxide (determined at the 50% of the maximum intensity of the substrate signal $SiOH^+$ at $m/z = 45$, similar to reference [25]).

Finally, polystyrene and poly(methyl methacrylate) standards for gel permeation chromatography (GPC) with relatively low molecular weight ($M_w$) of 1100 g/mol (($C_8H_8)_n$, ~10 repeating units) and 2180 g/mol (($C_5H_8O_2)_n$, ~21 repeating units), respectively, were purchased from Scientific Polymer Products Inc. (Ontario, USA) and Sigma-Aldrich Inc. (St. Louis, USA). These polymers will be referred to as *PS 1 k* and *PMMA 2 k*. Solutions of each polymer in toluene (Sigma-Aldrich, ≥ 99.71% purity) with a concentration of ~20 mg/mL were spin coated onto silicon wafers cleaned with isopropanol (same spin coating parameters as for Irganox 1010). The solutions were filtered using 0.2-μm Teflon filters to remove any non-dissolved particles and dust before their deposition on the silicon. The thickness of the polymer overlayers was in the range 50–70 nm. An overview of the samples employed in this study is reported in Table 1.

### 2.2. XPS analyses

XPS analysis was conducted in order to evaluate the thickness of the native oxide layer on the silicon substrate (subsequently introduced into the ellipsometric model of Section 2.3) based on the inelastic scattering theory [26]. Furthermore, the thickness of two Irganox 1010 ultrathin films of the series A-F described in Section 2.1, i.e. samples A and C, was assessed by XPS in order to qualitatively determine the depth at which the ion enhancement phenomenon is observed in SIMS molecular depth profiling. The XPS analyses were carried out with a SSX 100/206 photoelectron spectrometer from Surface Science Instruments (USA) equipped with a monochromatized micro-focused Al X-ray source (powered at 20 mA and 10 kV). The samples were fixed with double-sided conductive carbon tape onto an aluminium carousel. The pressure in the analysis chamber was around $10^{-6}$ Pa. The angle between the surface normal and the axis of the analyzer lens was 55°. The analyzed area was approximately 1.4 $mm^2$ and the pass energy was set at 50 eV. Under these conditions, the full width measured at half maximum (FWHM) of the Au 4f7/2 peak for a clean gold standard sample was around 1.1 eV. No charge compensation was applied as it was still possible to perform the measurements under conductive conditions without surface charging of

the sample and peak deformation. However, the binding energy scales were post adjusted for a few tenths of eV to set the Si 2p3/2 contribution of the metallic silicon at 99.0 eV. The same correction was extended to the corresponding C 1s and O 1s spectra. Data treatment was performed with the CasaXPS program (Casa Software Ltd, UK). Some spectra were decomposed using the least squares fitting routine provided by the software with a Gaussian/Lorentzian (85/15) product function and after subtraction of a non-linear baseline. Molar fractions were calculated using peak areas normalized based on acquisition parameters and sensitivity factors provided by the manufacturer. The details of the XPS calculations are reported in the supporting information.

### 2.3. Ellipsometry and profilometry

A spectroscopic ellipsometer (WVASE M-2000, J.A.Woollam Inc, USA) was used to measure the thickness of the Irganox 1010 single-layers on silicon substrates, in the wavelength range 400–800 nm (in most cases except when the depolarization factor exceeded 20%) with intervals of 1 nm at incidence angles of 65 and 70°. The measurements were carried out at 2 different points on each sample to obtain an average thickness. The data acquisition and consecutive modelling were performed with the CompleteEase 5.04 software. The model consisted of a standard Si substrate covered with a fixed 1.3-nm $SiO_2$ layer (on the basis of XPS data), followed by a Cauchy dispersion layer used to represent the Irganox film. The $n$ and $k$ values used for both the Si substrate and the $SiO_2$ were provided by the software database and kept constant throughout the modelling procedure. The $A$ and $B$ parameters of the top Cauchy layer along with its thickness $d$, was allowed to be fitted freely and simultaneously. The sputtered depths and the crater sizes were measured by a stylus profilometer DektakXT (Bruker Nano Surfaces Division, Tucson AZ, USA) in 3D imaging mode with a 0.7-μm radius tip over a field of view of 1500 × 1500 $μm^2$ and applying a force of 0.3 mg.
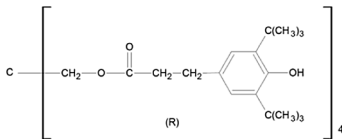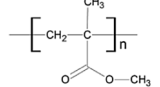
### 2.4. ToF-SIMS analyses

The time-of-flight (ToF)-SIMS experiments were performed using a TOF.SIMS 5 (IONTOF GmbH, Münster, Germany) instrument equipped with both Bi(Mn) Nanoprobe-LMIG (liquid metal ion gun) and Ar-GCIB (gas cluster ion beam) primary ion sources providing beams oriented at 45° to the surface normal. The Ar cluster source is equipped with a 90° pulsing system for mass separation by momentum deflection [27]. The pulsing system also allows the variation of the applied cluster size out of the large cluster size distribution, ranging from 250 to 10 000 atoms. The secondary ions are extracted using a potential of 2 kV into a reflectron-type ToF analyzer in the direction perpendicular to the sample surface.

SIMS molecular depth profiles were acquired both in positive and negative ion polarities on freshly prepared thin films. A DC 10-keV $Ar_{3000}^+$ ion beam (0.4 nA) was employed to sputter a 1000 × 1000 $μm^2$

**Table 1**
List of the different organic overlayers investigated in this study.

| Overlayer | Chemical structure | Substrate |
|---|---|---|
| 1) Irganox 1010 | | Si<br>PET<br>(PET chemical structure) |
| 2) PS 1 k | | Si |
| 3) PMMA 2 k | | Si |

area for all the experiments. The use of a 20 eV electron flood gun (25 μA) for charge compensation during depth profiling was necessary on insulated specimens. High mass resolution profiles (reference) were obtained in non-interlaced dual ion beam mode [28] by collecting the mass spectra from a $500 \times 500 \, \mu m^2$ area, concentric to the sputtered surface, with a pulsed beam of 30-keV $Bi_5^+$ ions (0.04 pA). The 30-keV $Bi_5^+$ mass spectra reconstructed from the bulk region of the Irganox 1010 profiles show a mass resolving power at $m/z$ 1176 ($M^+$) of around 5000, which is sufficient to resolve the hydrocarbon from the O-containing ions in the low $m/z$ region. Additionally, Ar-GCIB depth profiles were performed by using the same GCIB column alternately as an analysis gun (AC beam) and as a sputter gun (DC beam). Here, a settle time of 10 s was applied before each analysis and sputtering sequences in order to ensure an equilibrium current. For the analysis beam, four different cluster sizes were produced in order to study the effect of the $E/n$. Therefore, differential accumulation times were set for each $Ar_n^+$ analysis beam to partly compensate for considerable differences in primary ion current. Charge neutralization during utilization of both analysis and sputtering ion guns was required in this depth profiling mode. Two depth profiles were acquired per ion polarity in most analytical conditions on the same sample, showing high reproducibility of the measurements. GCIB spectra are characterized by poorer mass resolving power with respect to the 30-keV $Bi_n^+$ ion beam used for reference, which not only prevents the isotope peaks from being separated but also the hydrocarbon from the oxygenated ions in the low $m/z$ region of O-containing compounds such as Irganox 1010 and PMMA. For instance, $m/\Delta m = 750$ for $1176^+$ and $m/\Delta m = 650$ for $1175^-$ of the Irganox 1010 mass spectra from the bulk region of the profile obtained with an 10-keV $Ar_{1500}^+$ analysis beam. Finally, sputter yield volume measurements were conducted for two different sputter sizes, i.e. $n = 1500$ and $n = 5000$. The different depth-profiling conditions used in this work are summarized in Table 2, whereas the target currents and the raster area for each ion beam used are reported in Table 3.

Finally, SIMS spectra were acquired on Irganox 1010 thin films with increasing thickness (1–50 nm), both with a 30-keV $Bi_5^+$ ion beam and a 10-keV $Ar_{1500}^+$ ion beam. All the mass spectra were recorded from a $500 \times 500 \, \mu m^2$ area on the same sample, with no charge compensation since the coatings were sufficiently thin to avoid any detectable charging effect on the data (samples were grounded). The total ion dose was $9.6 \times 10^9$ ions/cm² for 30-keV $Bi_5^+$ and $2.2 \times 10^{10}$ for 10-keV $Ar_{1500}^+$, which ensured static bombardment conditions. Three measurements per polarity were performed for each sample. The mass resolving power at $m/z$ 1176 ($M^+$) for the 10-keV $Ar_{1500}^+$ analysis beam in this experiment was 1400, allowing the discrimination (but not the full separation) of the two first C13-contributions, namely $^{13}CC_{72}H_{108}O_{12}^{+\cdot}$ ($m/z$ 1177) and $^{13}C_2C_{71}H_{108}O_{12}^{+\cdot}$ ($m/z$ 1178). Instead, the 30-keV $Bi_5^+$ spectra present a mass resolving power of 5000 ($m/z$ 1176), which permits the clear separation between $C_{73}H_{108}O_{12}^{+\cdot}$ ($M^+$) and all the C13-isotope peaks until $^{13}C_4C_{69}H_{108}O_{12}^{+\cdot}$ at $m/z$ 1180. In order to account for the differences in mass resolving power between different analysis beams ($Bi_5^+$ vs $Ar_n^+$) and Ar-GCIB analysis modes (spectra vs profiles), the integration limits for the Irganox 1010 characteristic fragment ions with $m/z > 500$ include all the C13-contributions separable by the bismuth beam.

Since the aim of this study is also to compare different materials (Table 1), in positive polarity $SiOH^+$ ($m/z$ 45) is replaced by $Si^+$ ($m/z$ 28) ion signal for the determination of the interface with the organic overlayers because of severe spectral interference upon 10-keV $Ar_n^+$ analysis with $CHO_2^+$ and $C_2H_5O^+$ which are surface contaminants (but also PMMA fragments, the other material investigated in this work). Instead, in negative ion polarity the ion $HSiO_3^-$ is used for the location of the interface with the silicon substrate.

## 3. Results and discussion

The positive and negative fragment ions of Irganox 1010 investigated in this study are reported in Fig. 1, in addition to the (quasi-)molecular ions $C_{73}H_{108}O_{12}^{+\cdot}$ at $m/z$ 1176 and $C_{73}H_{107}O_{12}^-$ at $m/z$ 1175.

30-keV $Bi_5^+$ ions and 10-keV $Ar_{1500}^+$ ions were used alternatively to analyze the bottom of a crater made by a 10-keV $Ar_{3000}^+$ beam on Si-supported Irganox 1010 films of $\sim 50$-nm thickness (Si cleaned with isopropanol). The resulting molecular depth profiles acquired in the negative ion mode, which is preferred for the detection of an intense molecular ion signal $(M-H)^-$, $C_{73}H_{107}O_{12}^-$, are shown in Fig. 2a for the 30-keV $Bi_5^+$ analysis and in Fig. 2c for the 10-keV $Ar_{1500}^+$ analysis. The substrate signal used to determine the interface position is $HSiO_3^-$ at $m/z$ 73, because of its high intensity and minimal interference with Irganox 1010 fragments or surface contaminants. In the 30-keV $Bi_5^+$ profile of Fig. 2a, the characteristic ions present a slight signal rise at the interface with the Si substrate which is even more important for bigger fragments such as $C_{56}H_{83}O_{10}^-$ ($CR_3$-$CH_2$-$O^-$, not shown) and $(M-H)^-$. A similar observation was made by Green et al. [15] in reconstructed depth profiles acquired with a 25-keV $Bi_3^+$ analysis beam and a 10-keV $C_{60}^+$ sputter beam on Irganox 1010 thin films deposited on silicon. Green et al. demonstrated that such a rise in molecular secondary ion intensity is not correlated with the concentration of adventitious sodium that tends to accumulate at the interface due to surface charging [15 and references therein]. This might not be the case at higher concentrations of Na, for instance in biological samples, that could influence the ionization efficiency of the molecule, determining variations of the secondary ion yields (matrix-enhanced SIMS [29]). In contrast, the depth profiles performed with 10-keV $Ar_n^+$ analysis beams are always characterized by a strong rise of all ion signals at the interface with the substrate as depicted in Fig. 2c (in this case, 10-keV $Ar_{1500}^+$ analysis). It is also worth noticing that the profiles acquired with a 10-keV $Ar_{1500}^+$ analysis beam show a true plateau without any substantial intensity changes in the initial (transient) region, suggesting that the sputtering yield volume is sufficiently high to remove enough damaged material by the sputter beam so that an equilibrium is established [30]. In this paper, the central region of the profiles characterized by constant ion signals (plateau) will be referred to as the 'bulk region' of the thin film under investigation, and it will be used for determining the (relative) signal enhancement observed at the interface.

In order to confirm the enhancement effect present in the Ar-GCIB depth profiles of Si-supported Irganox 1010 single-layers, a second experimental approach was attempted. To this purpose, Irganox 1010 films on Si of different thicknesses ranging from (sub)-monolayers to $\sim 50$ nm

**Table 2**
Experimental conditions for ToF-SIMS depth profiling.

| 30-keV analysis beam | | 10-keV sputter beam | E/n (eV/atom) | Comment |
|---|---|---|---|---|
| $Bi_5^+$ | | $Ar_{3000}^+$ | 3.3 | Reference profile |

| 10-keV analysis beam | E/n (eV/atom) | 10-keV sputter beam | E/n (eV/atom) | Comment |
|---|---|---|---|---|
| $Ar_{800}^+$ | 12.5 | $Ar_{3000}^+$ | 3.3 | Study of the effect of Ar cluster size (in analysis) |
| $Ar_{1500}^+$ | 6.7 | | | |
| $Ar_{3000}^+$ | 3.3 | | | |
| $Ar_{5000}^+$ | 2.0 | | | |

| 30-keV analysis beam | | 10-keV sputter beam | E/n (eV/atom) | Comment |
|---|---|---|---|---|
| $Bi_5^+$ | | $Ar_{1500}^+$ | 6.7 | Y calculation |
| | | $Ar_{5000}^+$ | 2.0 | Y calculation |

**Table 3**
Target current of the different ion beams used in SIMS depth profiling.

| 30-keV analysis beam | Current (pA) | 10-keV sputter beam | Current (nA) |
|---|---|---|---|
| $Bi_5^+$ | 0.04 | $Ar_{3000}^+$ | 0.40 |
|  | Raster: $500 \times 500$ um² |  | Raster: $1000 \times 1000$ um² |
| **10-keV analysis beam** | **Current (pA)** | **10-keV sputter beam** | **Current (nA)** |
| $Ar_{800}^+$ | 0.02 | $Ar_{3000}^+$ | 0.40 |
| $Ar_{1500}^+$ | 0.07 |  |  |
| $Ar_{3000}^+$ | 0.04 |  |  |
| $Ar_{5000}^+$ | 0.007 |  |  |
|  | Raster: $500 \times 500$ um² |  | Raster: $1000 \times 1000$ um² |
| **30-keV analysis beam** | **Current (pA)** | **10-keV sputter beam** | **Current (nA)** |
| $Bi_5^+$ | 0.04 | $Ar_{1500}^+$ | 0.10–0.03 |
|  | 0.04 | $Ar_{5000}^+$ | 0.10–0.03 |
|  | Raster: $200 \times 200$ um² |  | Raster: $600 \times 600$ um² |

(total thickness of the films previously profiled: see Fig. 2a,c) were made by spin-coating. Surface analysis was performed on each sample with both 30-keV $Bi_5^+$ and 10-keV $Ar_{1500}^+$ beams, this time without charge compensation as the specimens are grounded. The intensities of the characteristic fragment ions followed in the profiles of Fig. 2a,c are now plotted as a function of the concentration of the spin-coated solution in Fig. 2b for 30-keV $Bi_5^+$ and Fig. 2d for 10-keV $Ar_{1500}^+$, mimicking a traditional depth profiling experiment. The analysis dose was kept constant for all the spectra, thus no further normalization is required to compare the intensities recorded on the different films. The signal of the silicon substrate is illustrated to verify the sub-monolayer nature of the thinnest coating. Fig. 2b (right) reproduces the traditional depth profile relatively well, performed with 30-keV $Bi_5^+$ analysis and depicted on Fig. 2a (left): the relative secondary ion intensities are respected, as well as the significant signal rise of the ion $(M-H)^-$ with a maximum at 3.8 nm from the silicon support (see XPS calculation for sample C in supporting information). The same conclusion can be drawn for the 10-keV $Ar_{1500}^+$ analysis beam (Fig. 2c versus d). It is worth noticing that also the relative positions of the maxima near the interface of Fig. 2c are found in the reconstructed profile of Fig. 2d, when they are sufficiently separated such

as in the case of the ions $(M-H)^-$ in green and $C_{17}H_{25}O_3^-$ in yellow. The smaller $C_{17}H_{25}O_3^-$ ion is essentially one of the four identical arms of the Irganox 1010 molecule (see Fig. 1). The intensity ratio between the two ions varies at the interface in the depth profile of Fig. 2c in favor of $(M-H)^-$. The higher increase of the quasi-molecular ion compared to $C_{17}H_{25}O_3^-$ (a fragment of the entire molecule) cannot be ascribed purely to a fragmentation effect at the interface since it would determine the opposite trend (the fragment ion intensity should increase to the expenses of the molecular ion signal). This would be rather influenced by changes in the charge transfer processes determining the ion formation when approaching the interfacial region. However, a more complex combination of the two effects cannot be excluded. This will be the subject of study in the present paper. Finally, the protocol using thin films of increasing thickness demonstrates the validity of the depth profiling approach used in this study to assess the molecular ion yield enhancement at the interface. The latter presents a series of advantages, such as the removal of surface contamination in addition to the possibility to cover a large spectrum of beam conditions with a limited number of samples. The comparison of the two different methodologies allows us to exclude major chemical damage issues related to the sputtering of the specimen and its exposure to electron
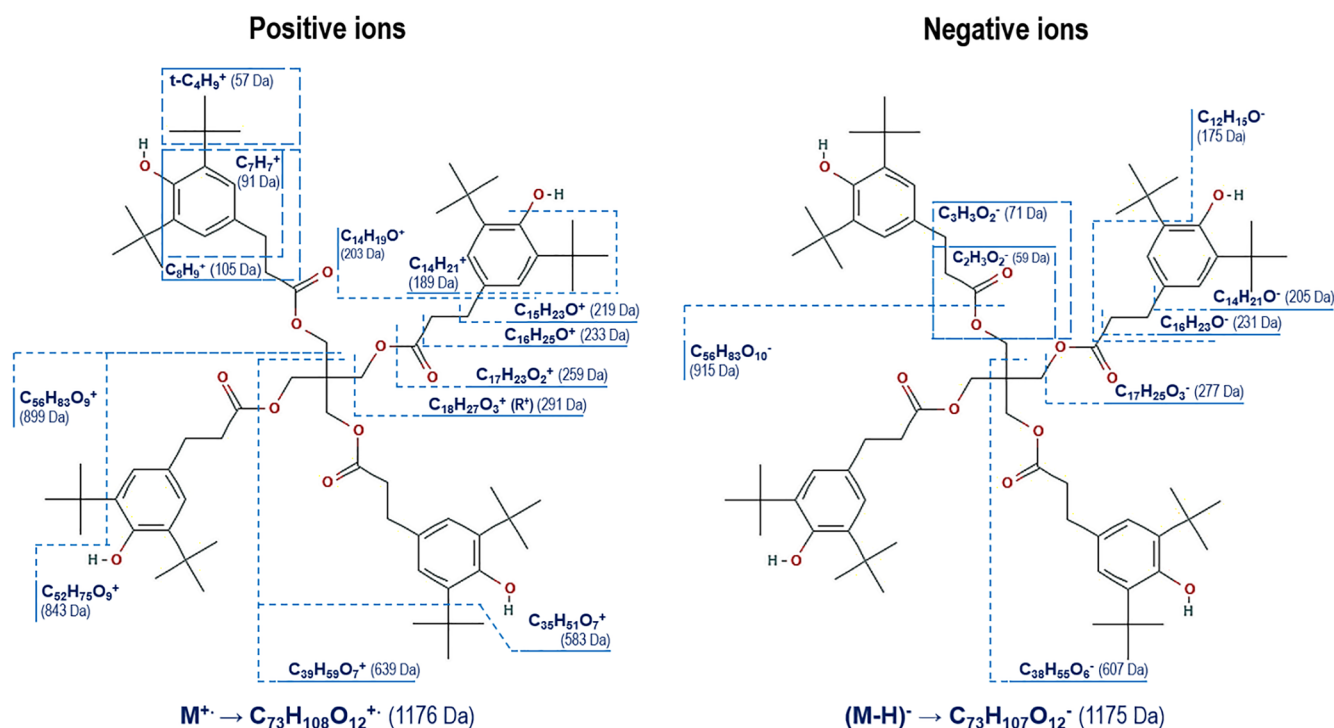


**Fig. 1.** Characteristic fragment ions of Irganox 1010 in positive polarity (left) and negative polarity (right). $C_{73}H_{108}O_{12}^{+\cdot}$ (*m/z* 1176) and $C_{73}H_{107}O_{12}^-$ (*m/z* 1175) are respectively the positive and negative molecular ions.
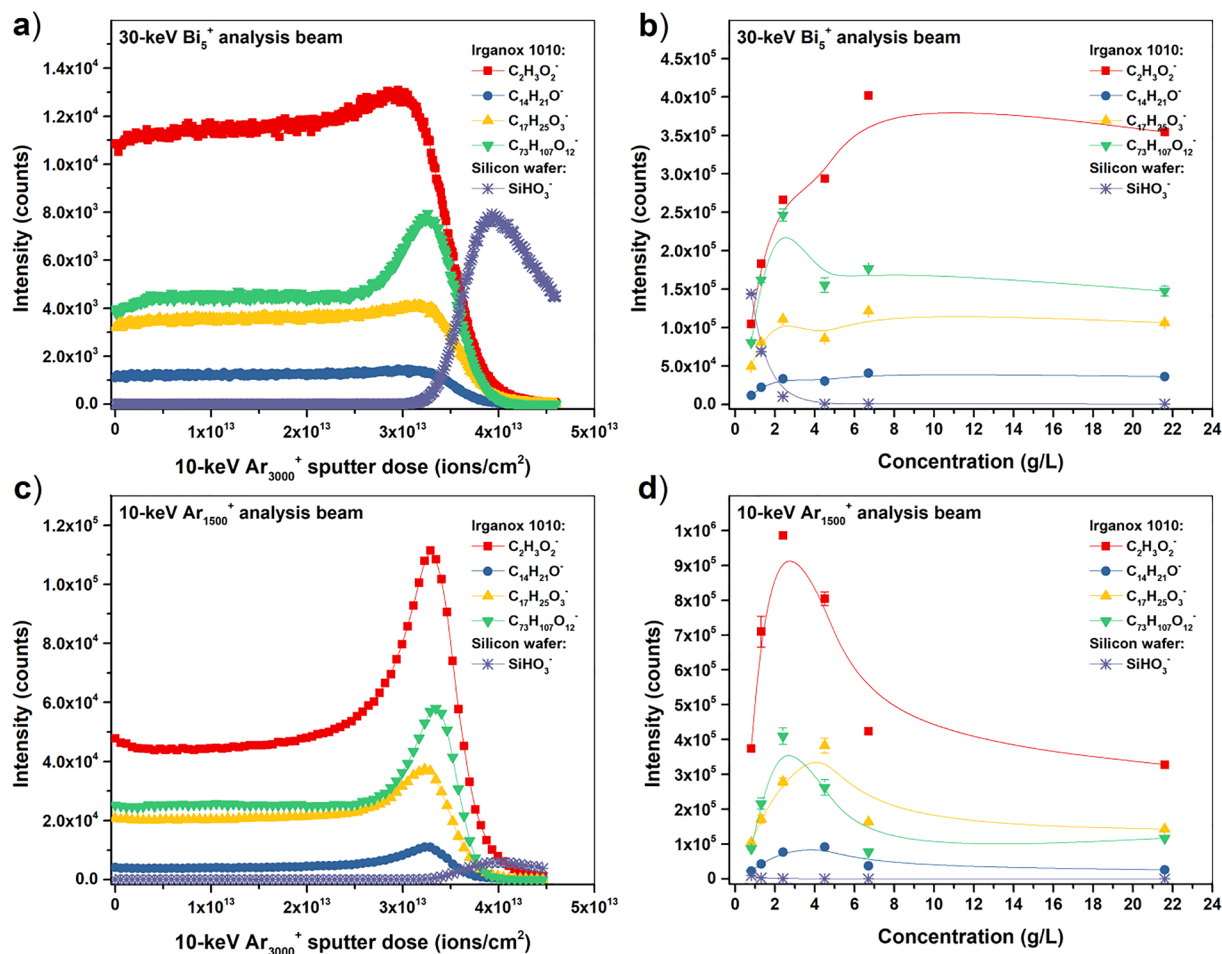
**Fig. 2.** Negative ion depth profiles of an Irganox 1010 film on silicon substrate acquired with a 30-keV $Bi_5^+$ (a) and 10-keV $Ar_{1500}^+$ analysis beam (c), respectively, and a 10-keV $Ar_{3000}^+$ sputter beam. Evolution of the intensities of the characteristic negative ions of Irganox 1010 overlayers on silicon as a function of the concentration of the spin-coated solution when a 30-keV $Bi_5^+$ (b) or a 10-keV $Ar_{1500}^+$ analysis beam (d) is employed. The trend of each secondary ion detected in depth profiling mode (a,c) is similar to that obtained with a different protocol using thin films of different thickness (b,d).

beam doses (charge neutralization) far in excess of the recommended limit of $6 \times 10^{18}$ electrons/m² for static SIMS [31–33].

The observed enhancement effect for the Irganox 1010 at the interface with the silicon substrate might be explained by the concomitance of the following factors: 1) ionization changes in the interfacial region; 2) fragmentation changes in the ultrathin layer regime; and 3) sputtering increases when the overlayer thickness decreases, as was demonstrated experimentally [20] and modelled by MD simulations on similar systems [34]. The next sections of this paper will consider each of the presented hypotheses consecutively.

### 3.1. Positive ions

In order to investigate the influence of ionization changes on the observed phenomenon, depth profiles were performed in the opposite ion polarity, i.e. positive, on the same Irganox 1010 sample with the 30-keV $Bi_5^+$ (Fig. 3a) and 10-keV $Ar_{1500}^+$ analysis beams (Fig. 3c), respectively, and the 10-keV $Ar_{3000}^+$ beam for sample etching. Our hypothesis here is that, if variations of the charge exchange processes are dominant, the evolutions of negative and positive ions might reveal important differences, as was previously observed in the case of organic photovoltaic layers near the interface with the inorganic substrate [35]. As anticipated in Section 2.4, the $Si^+$ ion signal will be used further on in the text for the location of the interface instead of $SiOH^+$. One needs to bear in mind that the silicon wafer is covered by a ~1.3-nm native oxide layer (determined by XPS [36,37]), therefore the oxide-related

signals like $SiOH^+$ rise before that of $Si^+$ [15,20].

Once again, the intensities of the bigger fragment ions rise near the interface with the silicon wafer during 30-keV $Bi_5^+$ analysis (Fig. 3a), as observed for $C_{56}H_{83}O_9^+$ ($CR_3$-$CH_2^+$, solid triangles). Also the 10-keV $Ar_{1500}^+$ positive depth profile (Fig. 3c) presents signal enhancement for all the fragment ions, such as $C_{14}H_{21}^+$ (189⁺) and $C_{15}H_{23}O^+$ (219⁺), as was the case for the negative profile (Fig. 2c). Both positive profiles were reproduced satisfactorily with the surface analysis protocol by using films of increasing thickness, as shown in Fig. 3b,d.

The observation of the enhancement at the interface in both negative and positive ion modes suggests that ionization is not the only cause of the observed effects. Nevertheless, the enhancement seems much more pronounced in the negative ion mode for 10-keV $Ar_{1500}^+$ analysis. Therefore, a contribution of ionization/matrix effects is probable. Finally, the substrate signal recorded on the Irganox 1010 (sub-)monolayers under different analysis conditions shows a certain variability (Fig. 3b,d and Fig. 2b, d) which is not primarily related to the different sampling depths of the two ion probes used [38,39], i.e. 30-keV $Bi_5^+$ and 10-keV $Ar_{1500}^+$, but rather to the inhomogeneity of the coating. However, this coverage effect, which determines a general diminution of the secondary ion intensities, does not completely prevent the enhancement effect from being observed.

### 3.2. Fragmentation

Previous studies have demonstrated that the distribution of ionized fragments emitted from organic surfaces under Ar cluster bombardment
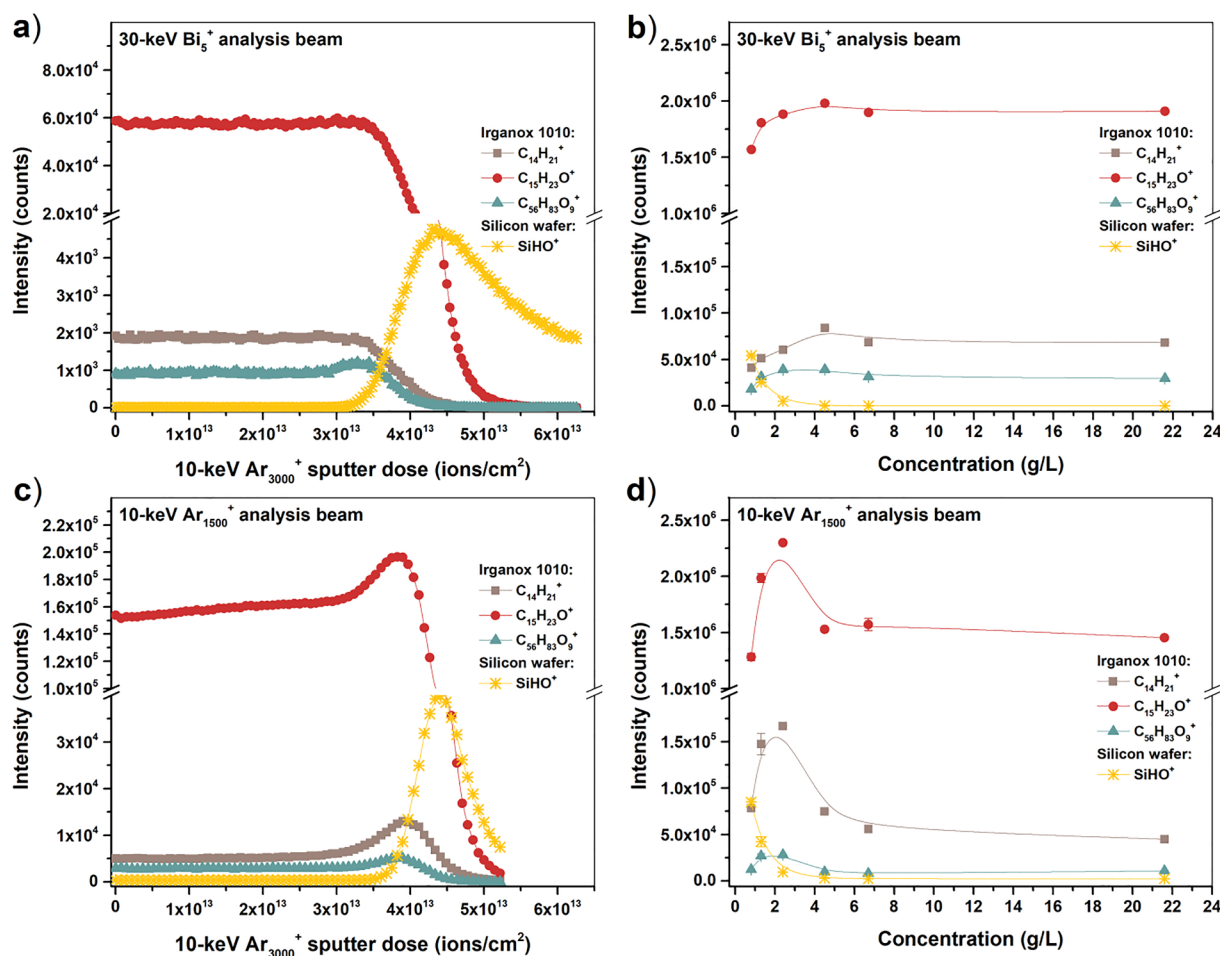
**Fig. 3.** Positive ion depth profiles of an Irganox 1010 film on silicon substrate acquired with a 30-keV $Bi_5^+$ (a) and 10-keV $Ar_{1500}^+$ analysis beam (c), respectively and a 10-keV $Ar_{3000}^+$ sputter beam. Evolution of the intensities of the characteristic positive ions of Irganox 1010 overlayers on silicon as a function of the concentration of the spin-coated solution when a 30-keV $Bi_5^+$ (b) or a 10-keV $Ar_{1500}^+$ analysis beam (d) is employed. The trend of each secondary ion detected in depth profiling mode (a,c) is similar to that obtained with a different protocol using thin films of different thickness (b,d).

were dependent on the scaled energy $E/n$ of the impinging cluster [40]. Therefore, in order to understand possible variations of fragmentation in the ultrathin layer regime, it is also useful to capture the $E/n$ dependence of the observed enhancement for a series of characteristic fragment ions. For this purpose, depth profiles of Irganox 1010 layers ($\sim 50$ nm) on silicon were acquired by 10-keV $Ar_n^+$ analysis beams of four different cluster sizes $n = 800, 1500, 3000,$ and 5000 atoms ($E/n$ [eV/atom] = 12.5, 6.7, 3.3, and 2), as shown in Table 2. In all the experiments, the etching was performed by 10-keV $Ar_{3000}^+$ ions. In-depth measurements were done with both ion polarities. First, the steady state region of each depth profile was identified to reconstruct the corresponding bulk mass spectrum, which was then normalized by the corresponding primary ion current. The secondary ion yields (counts/primary ion (PI)) were then plotted as a function of $E/n$ as depicted in Fig. 4 (black symbols). The evolution of the yields can now be compared with similar data sets that are found in literature as obtained with different experimental protocols. Fig. 4 illustrates the results of Kayser et al. [27] on surface analysis of thick Irganox 1010 films preceded by a gentle cleaning with a 5-keV $Ar_{2500}^+$ beam (0.5 nA, $700 \times 700\ \mu m^2$, 40 s) to minimize the surface contamination and to establish a better comparability [41]. The yields calculated by Kayser et al. (red symbols in Fig. 4) refer to an ion energy of 20 keV and $1000 \le n$ (atoms/cluster) $\le 10\ 000$ ($n = 500$ is omitted here). However, the two data sets can be compared in terms of the $E/n$ ratio [42,43], showing rather good agreement in the given ion yield evolutions. Indeed, the ion yields for the deprotonated molecular ion

$C_{73}H_{107}O_{12}^-$ and $C_{38}H_{55}O_6^-$ ($CR_2 = CH^-$ at $m/z$ 607) increase with decreasing $E/n$ (or increasing $n$) until reaching a maximum at $E/n = 8$ eV/atom (or 2500 atoms/cluster) for Kayser et al., which is similar in our case ($\sim 7$ eV/atom). Moreover, the $1175^-/607^-$ intensity ratio increases when increasing $n$, indicating a diminution of the fragmentation in both the surface and in-depth experiments. Thus, these ion yields decrease when decreasing $E/n$ or increasing $n$. The higher yields at $E/n = 2$ in our data set could be ascribed to an inaccurate reading of the 10-keV $Ar_{5000}^+$ analysis current that is barely measurable and/or to a detrimental contribution of the sputter beam. None of these factors affects the results discussed in this paper because they are based on a comparison of the bulk-interface under the same beam conditions.

The methodology applied for the fragmentation study is the following. Fig. 5 describes how the ion signal enhancement (a) and the position of the bump (b) at the interface of a depth profile are defined in this work for a given ion. A Gaussian smoothing (% of FWHM: 30; number of cycles: 2) was applied to all profiles before processing, in order to reduce statistical noise especially for the largest $n$ values. Briefly, the signal enhancement for a given secondary ion (Fig. 5a) is described as the difference between the maximum of intensity (after normalization to 1) shown at the interface between the organic overlayer and the substrate (silicon in Fig. 5) and the intensity in the bulk region of the depth profile (averaged on several tens of data points). On the other hand, the position of the bump is defined as the difference in sputter dose (ions/cm$^2$) between the maxima of the given ion and that of $Si^+$ in positive polarity or $HSiO_3^-$ in negative polarity. Positive
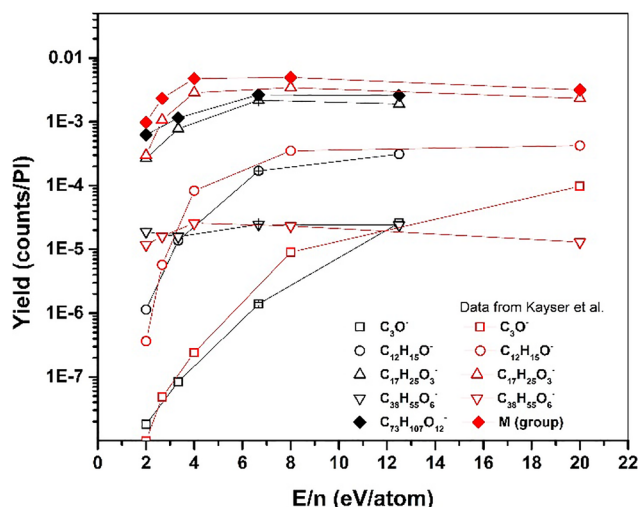
**Fig. 4.** Negative secondary ion yield in the bulk region of the 10-keV $Ar_n^+$ single beam depth profiles of Irganox 1010 as a function of $E/n$. Our data (black symbols) are compared with those from Kayser et al. [27] (red symbols) obtained with a different protocol, showing rather good agreement between the two data sets. (For interpretation of the references to color in this figure legend, the reader is referred to the web version of this article.)

*Δdose* values indicate that the bump is located before the maximum of the substrate signal, whereas negative values indicate the opposite. Prior to further experiments, the effect of the cleaning of the silicon substrate, i.e. ultra-sonication in organic solvent (isopropanol) versus Piranha-solution, was investigated on the Si-supported film of Irganox 1010 for a specific analysis condition that is 10-keV $Ar_{3000}^+$. The relative results (ion signal enhancement and shift at the interface) are reported in supporting information. In Fig. S4, it is apparent that the Piranha cleaning, although largely used for the removal of organic contamination, does not seem to be necessary in the present study. On the contrary, it has been observed that, if not properly carried out, the use of the Piranha solution introduces new sources of contamination such as sulphates $SO_x^-$, which will predominate in the Ar-GCIB spectra because of the higher surface sensitivity of argon clusters compared to the $Bi_n^+$ analysis ions. One also need to bear in mind that the low pH of the Piranha solution provokes the dissolution of inorganic deposits such

as metal oxides and carbonates, which alter the silicon surface in an uncontrolled manner. This is problematic when studying the interface. Therefore, it was decided to perform the cleaning of the silicon wafer with only organic solvents, and to carefully select the fragment ions that present any contributions from surface contaminants.

Fig. 6 shows the ion signal enhancements and the positions of the maximum intensity observed in the interfacial region for a series of characteristic ion fragments of an Irganox 1010 film on silicon (refer to Fig. 1 for the structure of the fragments), respectively, in the positive and negative ion polarities. In the negative polarity (c,d), the ions $25^-$, $41^-$, $49^-$ and $52^-$ are not strictly representative of the molecule being studied as they are the low mass ions $C_2H^-$, $C_2HO^-$, $C_4H^-$ and $C_3O^-$. However, all these peaks were chosen because they are mainly one-contribution peaks, and thus not problematic to work with the low $M/\Delta M$ of the GCIB analysis beams. In Fig. 6a,c, one can observe that, for all the considered ions, the intensity increases at the interface with the silicon substrate. In addition, the position of the bump becomes closer to the Si signal ($Si^+$ and $HSiO_3^-$) when the $m/z$ decreases as shown by the green symbols in Fig. 6b,d. Finally, when considering different cluster sizes for the $Ar_n^+$ analysis beam, the signal enhancements of all the reported ions increases as $E/n$ decreases or $n$ increases. For the smallest fragments, the intensity in the bulk drops to zero so that they are only detected in close proximity to the interface (enhancement equal to 1). On the other hand, the position of the intensity rise at the interface decreases as $E/n$ decreases. These two trends are clearly observed by the negative ion polarity in Fig. 6c,d.

The molecular ion $C_{73}H_{108}O_{12}^{+\cdot}$ involves only an electron loss to be formed (thus, no bond cleavage is involved). Therefore, if fragmentation were the only factor to be accounted for the observed enhancement effect at the interface, the ion $C_{73}H_{108}O_{12}^{+\cdot}$ should not display any changes in ion yield. However, this ion is showing a significant enhancement (0.28 with $Ar_{800}^+$) similarly to the other characteristic fragments considered in Fig. 6a, suggesting that ionization and/or sputtering variations might play a role too (in agreement with the observation done in Section 3.1). Angerer et al. have reported the depth profile of a 50-nm thick Irganox 1010 film on Si wafer acquired with a continuous 40-keV $Ar_n^+$ beam on the J105-3D Chemical Imager, where the $(M-H)^-$ is plotted [14] (the comparative data are reported in supporting information, Fig. S5). In those profiles, the pseudo molecular ion at $m/z$ 1175 shows a small bump just before the interface is reached under different analysis conditions, i.e. 40-keV $Ar_{4000}^+$,
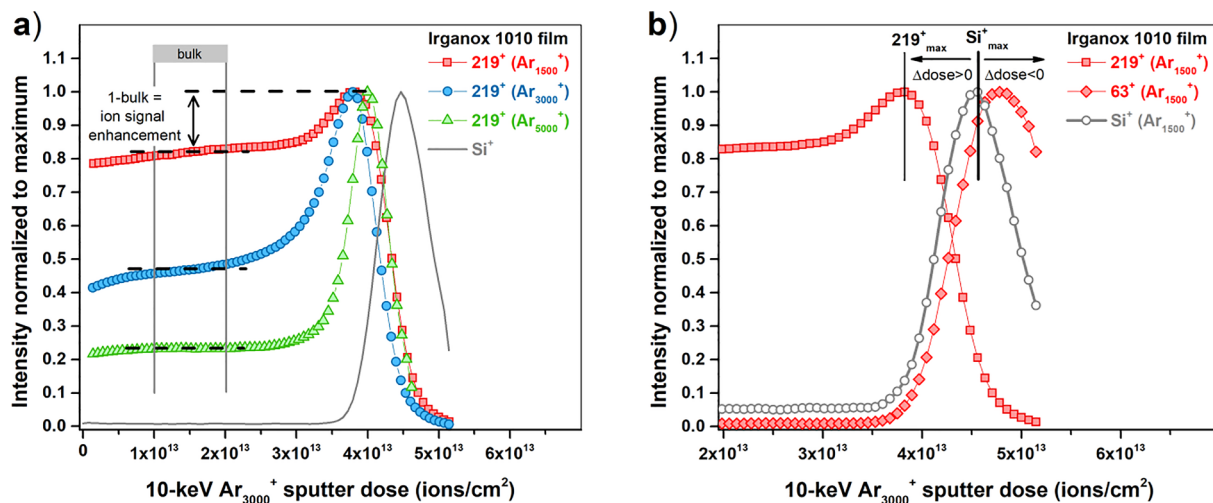


**Fig. 5.** (a) Definition of the ion signal enhancement for a given fragment as the difference between the maximum of intensity (after normalization to 1) shown at the interface between the organic thin film and the substrate (silicon in this case) and the intensity in the bulk region of a depth profile. Data smoothing is applied prior to analysis. (b) The position of the bump shown by the different fragment ions at the interface with the substrate is expressed as a difference in sputter dose between the maxima of the given ion and that of $Si^+$ in positive polarity, or $HSiO_3^-$ in negative polarity. Positive values indicate that the bump is located before the maximum of the substrate signal, whereas negative values describe the opposite case.
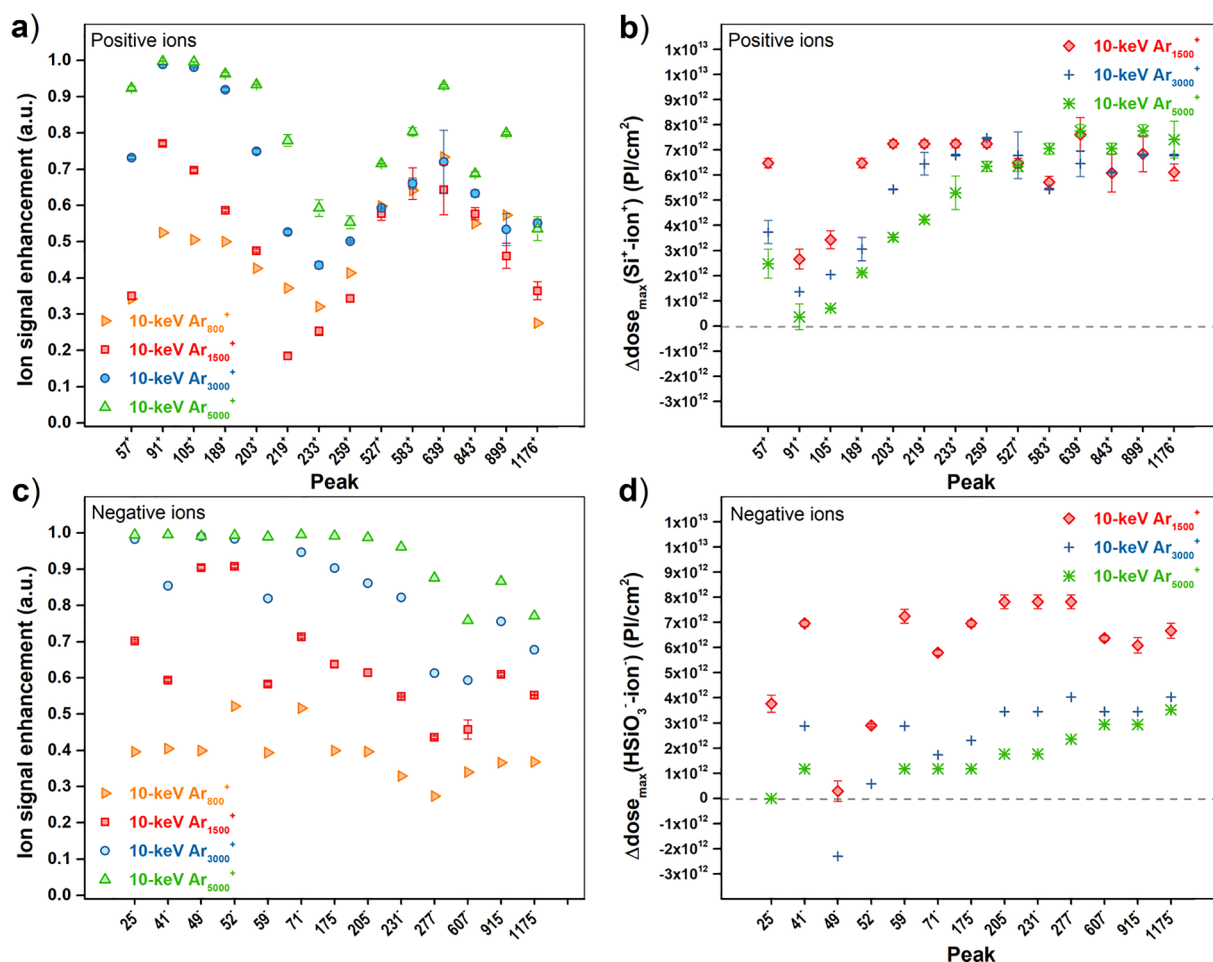
**Fig. 6.** Ion signal enhancement (a,c) and its location in relation to the substrate position (b,d) of characteristic fragments of Irganox 1010 films at the interface with the silicon wafer observed in depth profiling with four different 10-keV $Ar_n^+$ analysis beams (points with different colors). In all the experiments, the sputtering was performed by means of a 10-keV $Ar_{3000}^+$ ion beam. (For interpretation of the references to color in this figure legend, the reader is referred to the web version of this article.)

$Ar_{2000}^+$ and $Ar_{1000}^+$. These results are consistent with the present contribution, since the ion $(M-H)^-$ presents a significant signal enhancement when similarly analyzed by a 10-keV $Ar_{800}^+$ cluster beam both in analysis and sputter mode ($E/n = 12.5$ eV/atom), not shown here (resp. 40-keV $Ar_{4000}^+$).

In the positive ion polarity, a series of hydrocarbon ions $C_xH_y^+$ where the interference of the O-containing ions is minimal, have also been studied. Fig. 7 depicts the ion signal enhancement (a) and the position of the maxima at the interface (b) for small hydrocarbons up to $m/z$ 110, as a function of different $Ar_n^+$ cluster sizes (represented in different colors). The t-$C_4H_9^+$ ion is very characteristic of the Irganox 1010 since it is produced by the breaking of the (t-$C_4H_8)_2$-Phe- moiety contained in each of the four groups linked to the pentaerythritol core of the molecule. This explains its high intensity in the bulk of the different profiles and, consequently, the lowest values in Fig. 7a. Aromatic ions in each $C_x$ (x = 4–8) cluster are indicated in grey because of their singular behavior due to resonance stabilization, determining smaller enhancements [44]. Also, it is worth noticing that, with increasing cluster size of the $Ar_n^+$ analysis beam, the smallest ions of each $C_x$ series are no longer detected because of the limited fragmentation induced by the primary ions. This explains why the curves present fewer points with increasing *n*.

Fig. 7 shows a periodic variation of each $C_x$ (x = 1–8) ion series as a function of the H content: the signal enhancement increases when the H content decreases, as demonstrated for instance by the following series $C_7H_9^+ < C_7H_8^+ \leq C_7H_7^+$ (arom) $\ll C_7H_3^+$. Instead, in Fig. 7b, the

distance of the bump with respect to the silicon interface decreases as the H content decreases. In other words, in each $C_x$ (x = 1–8) series, the more the ions are fragmented or dehydrogenated, the *higher is the fraction* of the ion produced in the vicinity of the interface and the *closer to the silicon substrate* this ion will be generated. These sequences follow the internal energies needed to create the considered ions, $C_xH_y^+ \rightarrow C_xH_{y-n}^+$ ($n = 1, 2, …$). The more the initially saturated ion (ex. $C_7H_9^+$) is deprived of H atoms, the more internal energy it must have received. These systematic trends within the $C_xH_y^+$ (y = 2x-1) series when the number *y* of H atoms decreases was already observed in the broadening of the kinetic energy distributions (KEDs) measured on aliphatic and aromatic polyolefins by Delcorte et al. [45,46]. The phenomenological model considered an initial transfer of momentum and energy during the sputtering event, leading to the emission of a precursor hydrocarbon fragment, which was followed by a fast reorganization in the vicinity of the surface when the ion internal energy was in excess (in that case mainly consisting in H elimination to produce a less saturated ion). The threshold for the dehydrogenation process to occur was then given by the difference of formation energy between the original fragment and the reorganized fragment states. It was roughly proportional to the number of cleaved C-H bonds [45 and references therein]. In addition, it was evidenced by Cristaudo et al. by GCIB sputtering experiments [20] and Delcorte et al. by MD simulations [34], respectively, that the kinetic energy of the $Ar_n^+$ cluster deposited in the organic overlayer was partly confined at the interface with a harder substrate such as silicon due to its much higher stopping power,
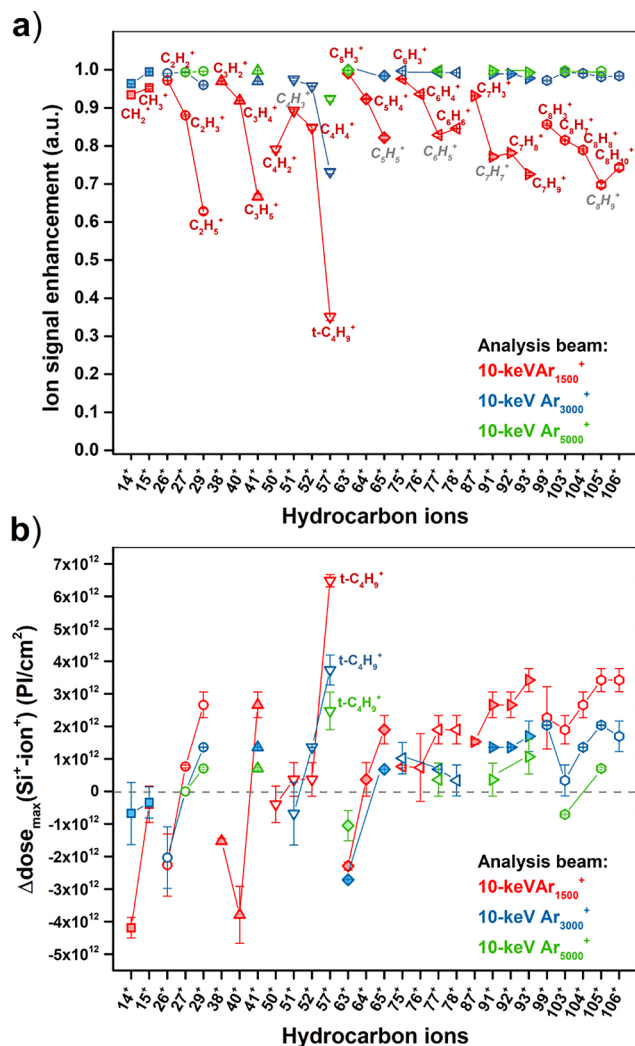
**Fig. 7.** a) Ion signal enhancement shown by hydrocarbon ions of Irganox 1010 films on silicon wafer observed in depth profiling with three different 10-keV $Ar_n^+$ analysis beams (curves with different colors). The aromatic ions are reported in grey. The t-$C_4H_9^+$ ion is a characteristic fragment of the Irganox 1010 molecule. b) Position of the maxima of the hydrocarbon signals in relation to the silicon substrate, as a function of the cluster size of the $Ar_n^+$ analysis beam. In all the experiments, the sputtering was performed by means of a 10-keV $Ar_{3000}^+$ ion beam. (For interpretation of the references to color in this figure legend, the reader is referred to the web version of this article.)

resulting in a significant increase of the sputtering yield in the interfacial region (see Section 3.3). In this region of the depth profile, dehydrogenated ions can be produced in a more efficient way due to the transfer of a larger amount of kinetic and internal energy (rotational and vibrational), which is directly released by fragmentation, resulting in an increased ion signal enhancement as the H/C ratio decrease. Additionally, the fraction of the ions produced at the interface as a function of the dehydrogenation should increase as one approaches the interface from the organic overlayer, following the gradient of the energy deposited by the ion projectile [47,48]. Therefore, in the $C_7$ series, for instance, this should determine a shift of the maximum signal at the interface in the following order $C_7H_9^+ > C_7H_8^+ \geq C_7H_7^+ > C_7H_3^+$. Also the effect of $E/n$ can be explained by the same arguments. Indeed, the ion signal enhancement increases when $E/n$ decreases because of more efficient energy confinement at the interface with the silicon (see t-$C_4H_9^+$). This is shown in Fig. 7b where the more fragmented (dehydrogenated) ions are generated in the very vicinity of the hard substrate.

Finally, saturation of the evolution of the ion signal enhancement as a function of $E/n$ for most of the $C_xH_y^+$ ions is already reached at a value of around 3 eV/atom (i.e. 10-keV $Ar_{3000}^+$), meaning that these fragments are produced uniquely at the interface. In other words, in the bulk region of the profiles the fragmentation threshold, i.e. the formation energy difference of the involved ion with respect to its precursor, is reached only with the 10-keV $Ar_{1500}^+$ analysis beam whereas in the other cases this happens exclusively at the interface due to energy nanoconfinement [20]. From Fig. 7 it is clear that the fragmentation at the interface constitutes a crucial factor in determining the intensity increase at the interface, as well as the maxima shifts. The role of the fragmentation is confirmed by the MD simulations conducted in Cristaudo et al. [20]. In this paper the model was a coarse grain representing an amorphous film of polyethylene-like oligomers. It has been calculated that under bombardment with 10 keV $Ar_{3000}$, the energy confinement effect starts causing fragmentation below 5 nm [unpublished data].

In order to check that the observed effects were not mainly sample-dependent, other materials were investigated such as PS 1 k and PMMA 2 k. Fig. 8 presents the comparison of the depth profiles for a thin layer of PS 1 k on silicon substrate acquired with a 30-keV $Bi_5^+$ and a 10-keV $Ar_{1500}^+$ analysis beam, respectively. $C_8H_9^+$ is the protonated monomer $(m + H)^+$ of polystyrene $(CH_2CH(C_6H_5))_n$, whereas $C_{16}H_{15}^+$ constitutes the deprotonated dimer $(2 m-H)^+$. For all the reported characteristic fragments of PS 1 k, one can see an intensity enhancement only in the profile recorded with the GCIB analysis beam (red-contour symbols), similar to the case of the Irganox 1010. Here, one can also find the maxima shifts at the interface – see that the smaller $C_6H_5^+$ is shifted more towards the $Si^+$ signal compared to larger fragments such as $C_{16}H_{15}^+$ (i.e. more internal energy is required to form $C_6H_5^+$). Fig. 8b illustrates the enhancement for a larger series of characteristic fragments of the polymer. Because of the oligomeric nature of the polystyrene used, it was possible to individuate the molecular weight distribution in the positive ion mass spectra and pick $C_{85}H_{91}^+$ as one of its most intense peaks. All the ions in the $m/z$ ranging from 12 to 1100 show a bump at the interface. Finally, as was the case for Irganox 1010, the ion signal enhancement increases with decreasing $E/n$ or increasing $n$, with the smallest fragments reaching saturation (enhancement equal to unit) at 3 eV/atom.

The interpretation of the polystyrene data is consistent with the discussion developed for Irganox. Ions such as $C_7H_7^+$, $C_8H_9^+$, $C_9H_9^+$, $C_{15}H_{13}^+$, $C_{16}H_{17}^+$ or $(2 m + H)^+$, $C_{85}H_{91}^+$ or $(M + H)^+$ present lower enhancements of around 0.5–0.6 as they are more PS-specific. Indeed, it has been determined by low and high energy collision-induced dissociation (CID) MS/MS studies [49] that fragment ions such as $C_8H_9^+$, $C_9H_9^+$ and $C_{15}H_{13}^+$ are derived directly from the main chain structure of the polymer, whereas ions such as $C_{10}H_8^+$ and $C_{13}H_9^+$ are related to cyclization reactions that occur at higher internal energies, explaining their enhanced formation in proximity to the interface (thus higher signal enhancement). It is worth noticing that t-$C_4H_9^+$ constitutes the end-group of PS 1 k, being synthesized by anionic polymerization, and thus representative of the polystyrene as well. This explains the different behavior of $C_4H_9^+$ with respect to other low $m/z$ fragments.

The results obtained on a PMMA 2 k thin film in both positive and negative polarities and in the $m/z$ range 0–200 are reported in the supporting information (Fig. S6, 10-keV $Ar_{1500}^+$ analysis beam). Fig. S6 shows a significant fragmentation near the surface for ions below $m/z$ 100 or the repeating unit $(C_5H_8O_2)_n$, while the enhancement is very little ($\leq 0.2$) for higher mass values. It could be hypothesized that the observed difference between PS 1 k and PMMA 2 k could be ascribed to the different degradation mechanism upon keV ion bombardment. In fact, PS mainly undergoes cross-linking reactions which determine an increase of the molecular weight that slows down the erosion, whereas PMMA principally undergoes chain scission and/or unzipping (depolymerization) reactions which favor the sputtering process [8,25,50].

Finally, the last hypothesis that needs to be evaluated concerns the
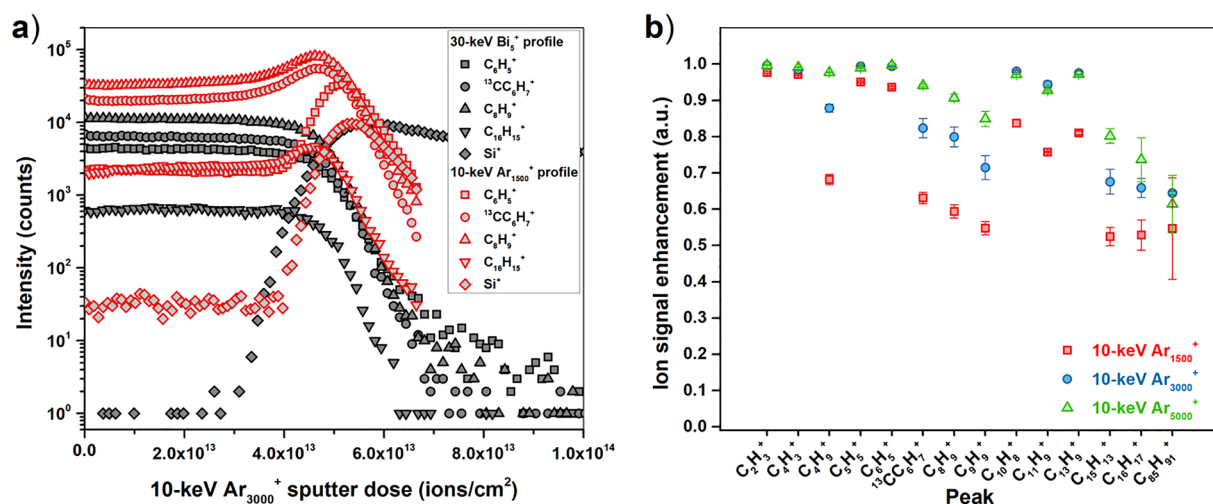
**Fig. 8.** a) Depth profiles of a silicon-supported PS 1 k film acquired with a 30-keV $Bi_5^+$ and a 10-keV $Ar_{1500}^+$ analysis beam, respectively. b) Ion signal enhancement of the characteristic fragments of the polystyrene oligomer (note that $C_{85}H_{91}^+$ represents one of the most intense peaks of the molecular weight distribution) shown at the interface with the silicon substrate when three different 10-keV $Ar_n^+$ analysis beams are used (n = 1500, 3000, 5000). In all the experiments, the sputtering was performed by means of a 10-keV $Ar_{3000}^+$ ion beam.

variation of the sputtering efficiency at the hybrid organic(soft)-inorganic(hard) interface. It will be presented in the next section.

### 3.3. Sputtering

In order to verify our last hypothesis concerning the effect of the sputtering variation on the signal enhancement at the interface (nanoconfinement effect [20]), we decided to repeat the Irganox 1010 experiments conducted in Section 3.1 (Figs. 2 and 3), on a soft PET substrate instead of silicon wafers. Fig. 9 depicts the positive (a,b) and negative (c,d) polarity profiles acquired with a 30-keV $Bi_5^+$ and a 10-keV $Ar_{1500}^+$ analysis beam, respectively. It is obvious that there is no signal enhancement for the most characteristic fragment ions of the Irganox 1010 molecule. The fact that the effect is only observed on hard substrates suggests that the sputtering must be playing an important role in the observed phenomenon.

Fig. 10 shows the enhancement of the sputter yield volume in the ultrathin film regime for Irganox 1010 overlayers on silicon wafer in two extreme sputtering conditions used in this work – 10-keV $Ar_{1500}^+$ ($E/n$ = 12.5 eV/atom) and 10-keV $Ar_{5000}^+$ ($E/n$ = 2 eV/atom). The experimental sputter yield enhancement factor SYEF is defined as $(Y_{\sim 10nm} - Y_{\sim bulk})/Y_{\sim 10nm}$ and it increases with decreasing $E/n$ from 0.35 for $Ar_{1500}^+$ to 0.55 for $Ar_{5000}^+$. This indicates that the energy confinement at the interface between a soft material and a hard substrate such as silicon becomes more efficient with decreasing $E/n$, explaining the effect of the $E/n$ on the ion signal enhancements and the relative locations of the bump with respect to the substrate illustrated in Fig. 6 and Fig. 7, respectively for the characteristic fragments and the small hydrocarbon ions $C_{1-8}$ of Irganox 1010 on silicon, and Fig. 8b for the PS1k film on silicon. Indeed, in a given profile the ion signal enhancements increase, and the maxima locate closer to the silicon substrate, as $E/n$ decreases. The variation of the sputter yield enhancement with $E/n$ is consistent with the trends of the universal sputtering curves, where the difference between the curves measured for organic materials (Irganox 1010) and inorganic materials (Si, SiO$_2$) increases significantly when $E/n$ decreases [42]. As MD studies show, the relative difficulty of larger Ar clusters to sputter inorganic materials directly relates to their energy per atom, becoming too low to dislocate the atoms from their lattice positions below a certain $E/n$ (around 2 eV for Si [51]). In that case, the energy transferred to the substrate diffuses via pressure waves and thermal excitation. In parallel, the backscattered energy fraction increases.

In order to compare the sputtering variations to the ion signal enhancements better, an average ion enhancement factor (AIEF) is defined as the average of the enhancements determined for the Irganox-specific (positive + or negative −) ion fragments taken into consideration in Section 3.2 (see Fig. 6). Even with the caveat that this AIEF parameter might not be fully representative because it is based on a selection of ions, it should help identify the major trends. The relative AIEF (+) and (−) values are reported in Table 4. Both AIEF (+) and (−) are consistently higher than SYEF (experimental and estimated at 3.8 nm), suggesting that the substrate provides a separate ionization enhancement for both ion polarities in addition to the sputtering increase explained by the energy nanoconfinement. Furthermore, the AIEF values are generally higher in the negative polarity compared to the positive one, indicating that this polarity is more subjected to ionization/matrix effects as already anticipated in Section 3.1 (Fig. 2 versus Fig. 3). Like SYEF, AIEF increases with decreasing $E/n$, and the ratio of the two factors does not vary much with varying cluster size (see $Ar_{1500}^+$ versus $Ar_{5000}^+$). The values reported in Table 4 for AIEF and SYEF estimated at 3.8 nm suggest that the sputter yield variations represent the major contribution to the average ion yield enhancement: ∼80% in the positive polarity and ∼70% in the negative polarity. However, beyond these average values, our results show a great diversity of behaviors for the different secondary ions, as was illustrated in Figs. 6 and 7 for Irganox, in Fig. 8 for PS and in Fig. S6 for PMMA. The origin of these distinct behaviors must be found in specific ionization and fragmentation mechanisms. In particular, the contribution of the fragmentation changes at the interface was demonstrated in Section 3.2 with hydrocarbon ions, for which the enhancement follows the increasing internal energy required for their formation. This "second order" effect is dramatic under $Ar_{5000}^+$ analysis, where most of the considered ions - absent in the bulk - start to be gradually produced when the interface is approached.

## 4. Conclusions

This study demonstrates the systematic enhancement of the ion signals in the interfacial region of the depth profiles of Irganox 1010 and PS 1 k films when using large argon clusters for analysis. For the first time, a correlation between the cluster size $n$ or energy per atom $E/n$ and the ion signal enhancement near the silicon substrate, as well as the maxima shifts, is established for both ion polarities. Three different hypotheses are formulated to explain the observed phenomenon, which
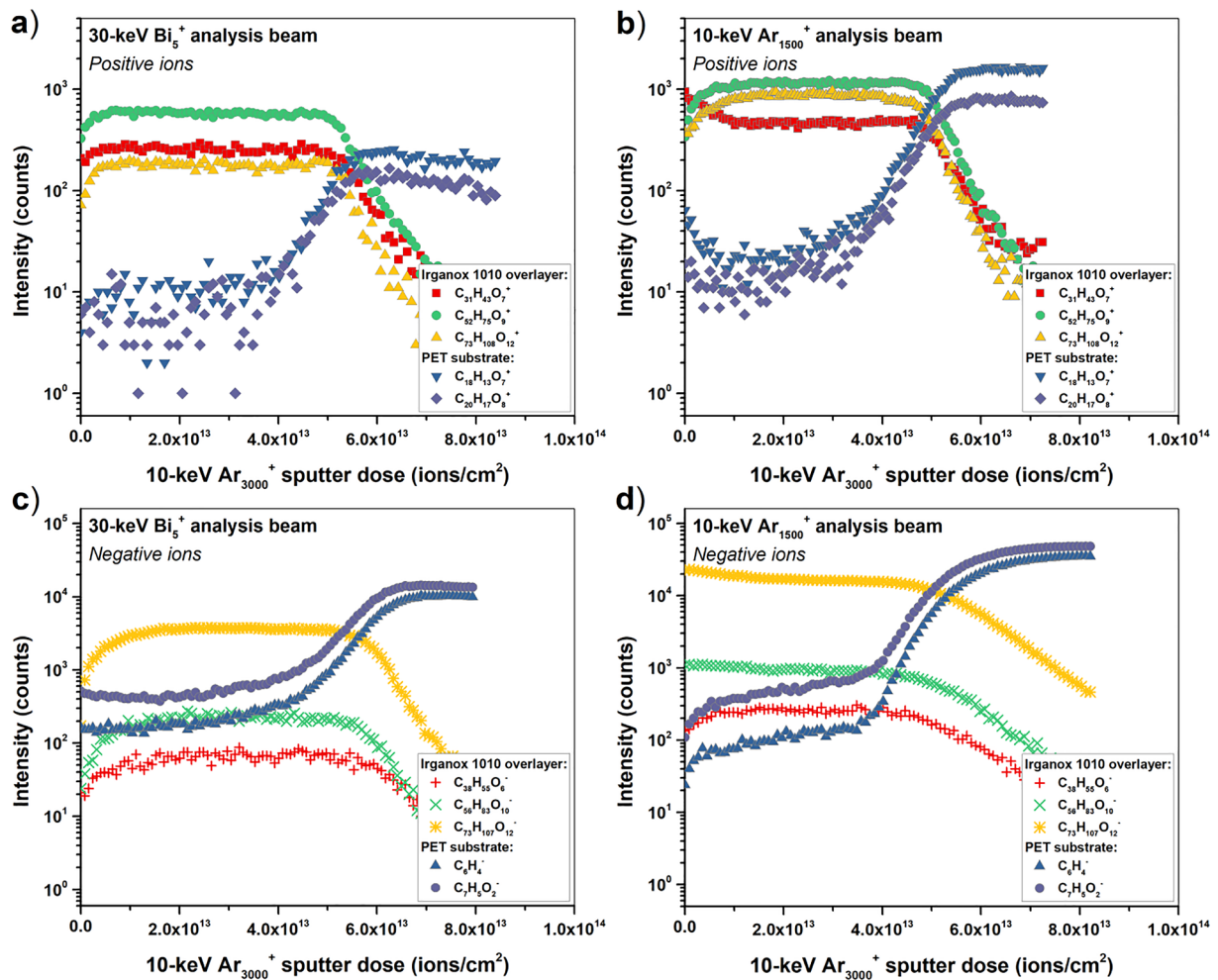
**Fig. 9.** Positive and negative ion depth profiles of an Irganox 1010 thin film deposited onto PET acquired with a 30-keV $Bi_5^+$ (a,c) and 10-keV $Ar_{1500}^+$ analysis beam (b,d), respectively. In all cases, a 10-keV $Ar_{3000}^+$ ion beam was employed to sputter the sample.
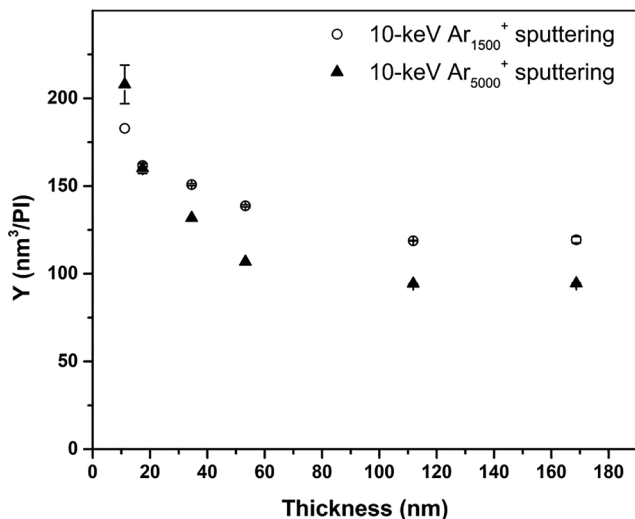


**Fig. 10.** Sputter yield volumes Y as a function of the thickness of Irganox 1010 films on silicon wafers for two distinct sputtering conditions, i.e. 10-keV $Ar_{1500}^+$ (open circles) and $Ar_{5000}^+$ (solid triangles). The sputtered volume of the two thickest overlayers is based on profilometry data of the measured craters.

**Table 4**
Average ion enhancement factors (AIEF) determined in both positive (+) and negative (-) polarity for the Irganox 1010 films on silicon wafer analyzed with different 10-keV $Ar_n^+$ beams (refer to Fig. 6). The sputter yield enhancement factors (SYEF) are reported in the two last column for two different analysis conditions: 10-keV $Ar_{1500}^+$ ($E/n$ = 12.5 eV/atom) and 10-keV $Ar_{5000}^+$ ($E/n$ = 2 eV/atom). The experimental SYEF refers to the measured values at around 10 nm, whereas the estimated SYEF refers to the maximum value achieved at 3.8 nm (bump location as determined by XPS).

| 10-keV $Ar_n^+$ analysis conditions | Irganox 1010 | | | |
|---|---|---|---|---|
| | AIEF (+) | AIEF (-) | SYEF (experimental) | SYEF (estimated) |
| $Ar_{800}^+$ | 0.48 ± 0.13 | 0.39 ± 0.07 | — | — |
| $Ar_{1500}^+$ | 0.50 ± 0.18 | 0.64 ± 0.14 | 0.35 | 0.43 |
| $Ar_{3000}^+$ | 0.68 ± 0.18 | 0.83 ± 0.14 | — | — |
| $Ar_{5000}^+$ | 0.80 ± 0.16 | 0.94 ± 0.09 | 0.55 | 0.66 |

advocate variations of sputtering and fragmentation at the organic–inorganic hybrid interfaces, as well as ionization/matrix effects. First, our measurements indicate that the sputtering yield increase in the

ultrathin regime constitutes a major contribution in the observed ion signal enhancements at the interface for Irganox 1010 films. It is also demonstrated that more fragmented ions are generated closer to the hard substrate. Additionally, this fragmented fraction increases with decreasing $E/n$ as the energy confinement increases. Finally, the sputtering and fragmentation changes are not the only variations that account for the ion enhancements in the interfacial region since also ionization/matrix effects intervene, especially in the negative polarity for the Irganox 1010 molecule. The concomitance of these different factors

makes the picture of the situation very complex. To further clarify the influence of ionization/matrix effects, future investigations should focus on systems known for ionization enhancement and suppression at the interface. A better understanding of ionization phenomena at the interface is important for the analyst, since the consequent apparent broadening or sharpening of the interface can lead to erroneous assessments of interface location, width and depth resolution of the SIMS molecular depth profiles.

## CRediT authorship contribution statement

**V. Cristaudo:** Conceptualization, Methodology, Investigation, Validation, Writing - original draft, Writing - review & editing. **C. Poleunis:** Methodology, Investigation. **P. Laha:** Investigation. **P. Eloy:** Investigation. **T. Hauffman:** Supervision. **H. Terryn:** Supervision. **A. Delcorte:** Conceptualization, Supervision, Funding acquisition.

## Declaration of Competing Interest

The authors declare that they have no known competing financial interests or personal relationships that could have appeared to influence the work reported in this paper.

## Acknowledgements

## Appendix A. Supplementary material

Supplementary data to this article can be found online at https://doi.org/10.1016/j.apsusc.2020.147716.

## References

[1] S. Ninomiya, K. Ichiki, H. Yamada, Y. Nakata, T. Seki, T. Aoki, J. Matsuo, Precise and fast secondary ion mass spectrometry depth profiling of polymer materials with large Ar cluster ion beams, Rapid Commun. Mass Spectrom. 23 (2009) 1601–1606.

[2] D. Rading, R. Moellers, H.-G. Cramer, E. Niehuis, Dual beam depth profiling of polymer materials: comparison of $C_{60}$ and Ar cluster ion beams for sputtering, Surf. Interface Anal. 45 (2013) 171–174.

[3] A. Delcorte, V. Cristaudo, M. Zarshenas, D. Merche, F. Reniers, P. Bertrand, Chemical analysis of plasma-treated organic surfaces and plasma polymers by secondary ion mass spectrometry, Plasma Processes Polym. 12 (2015) 905–918.

[4] T. Mouhib, C. Poleunis, R. Möllers, E. Niehuis, P. Defrance, P. Bertrand, A. Delcorte, Organic depth profiling of $C_{60}$ and $C_{60}$/phthalocyanine layers using argon clusters, Surf. Interface Anal. 45 (2013) 163–166.

[5] T. Mouhib, C. Poleunis, N. Wehbe, J.J. Michels, Y. Galagan, L. Houssiau, P. Bertrand, A. Delcorte, Molecular depth profiling of organic photovoltaic heterojunction layers by ToF-SIMS: comparative evaluation of three sputtering beams, Analyst 138 (2013) 6801–6810.

[6] C. Bich, R. Havelund, R. Moellers, D. Touboul, F. Kollmer, E. Niehuis, I.S. Gilmore, A. Brunelle, Argon cluster ion source evaluation on lipid standards and rat brain tissue samples, Anal. Chem. 85 (2013) 7745–7752.

[7] C.M. Mahoney, Cluster secondary ion mass spectrometry of polymers and related materials, Mass Spectrom. Rev. 29 (2009) 247–293.

[8] A. Delcorte, O.A. Restrepo, B. Czerwinski, Cluster SIMS of organic materials: theoretical insights, Cluster Secondary Ion Mass Spectrometry: Principles and Applications, first ed., John Wiley & Sons, New Jersey, 2013 Chapter 2.

[9] S.K. Wang, H.Y. Chang, Y.H. Chu, W.L. Kao, C.Y. Wu, Y.W. Lee, Y.W. You, K.J. Chu, S.H. Hung, J.J. Shyue, Effect of energy per atom (E/n) on the Ar gas cluster ion beam (Ar-GCIB) and $O_2^+$ cosputter process, Analyst 144 (2019) 3323–3333.

[10] N. Winograd, Gas cluster ion beams for secondary ion mass spectrometry, Annu. Rev. Anal. Chem. 11 (2018) 29–48.

[11] Q.P. Vanbellingen, N. Elie, M.J. Eller, S. Della-Negra, D. Touboul, A. Brunelle, Time-of-flight secondary ion mass spectrometry imaging of biological samples with delayed extraction for high mass and high spatial resolutions, Rapid Commun. Mass Spectrom. 29 (2015) 1187–1195.

[12] H.K. Shon, S. Yoon, J.H. Moon, T.G. Lee, Improved mass resolution and mass accuracy in TOF-SIMS spectra and images using argon gas cluster ion beams, Biointerphases 11 (2016) 02A321.

[13] M.K. Passarelli, A. Pirkl, R. Moellers, D. Grinfeld, F. Kollmer, R. Havelund, C.F. Newman, P.S. Marshall, H. Arlinghaus, M.R. Alexander, A. West, The 3D OrbiSIMS—label-free metabolic imaging with subcellular lateral resolution and high mass-resolving power, Nat. Methods 14 (12) (2017) 1175–1183.

[14] T.B. Angerer, P. Blenkinsopp, J.S. Fletcher, High energy gas cluster ions for organic and biological analysis by time-of-flight secondary ion mass spectrometry, Int. J. Mass Spectrom. 377 (2015) 591–598.

[15] F.M. Green, I.S. Gilmore, M.P. Seah, Cluster ion beam profiling of organics by secondary ion mass spectrometry–does sodium affect the molecular ion intensity at interfaces? Rapid Commun. Mass Spectrom.: Int. J. Devoted Rapid Disseminat. Up-to-the-Min. Res. Mass Spectrom. 22 (2008) 4178–4182.

[16] A.G. Shard, S.J. Spencer, S.A. Smith, R. Havelund, I.S. Gilmore, The matrix effect in organic secondary ion mass spectrometry, Int. J. Mass Spectrom. 377 (2015) 599–609.

[17] Y. Yamamoto, N. Shimodaira, SIMS depth profile analysis of sodium in silicon dioxide, Appl. Surf. Sci. 255 (2008) 860–862.

[18] A. Delcorte, P. Bertrand, Metal salts for molecular ion yield enhancement in organic secondary ion mass spectrometry: a critical assessment, Anal. Chem. 77 (2005) 2107–2115.

[19] R. Havelund, M.P. Seah, M. Tiddia, I.S. Gilmore, SIMS of organic materials-interface location in argon gas cluster depth profiles using negative secondary ions, J. Am. Soc. Mass Spectr. 29 (2018) 774–785.

[20] V. Cristaudo, C. Poleunis, A. Delcorte, Effect of nanoconfinement on the sputter yield in ultrathin polymeric films: experiments and model, Appl. Surf. Sci. 444 (2018) 780–788.

[21] C.B. Walsh, E.I. Franses, Ultrathin PMMA films spin-coated from toluene solutions, Thin Solid Films 429 (2003) 71–76.

[22] D. Ennis, H. Betz, H. Ade, Direct spincasting of polystyrene thin films onto poly (methyl methacrylate), J. Polym. Sci., Part B: Polym. Phys. 44 (2006) 3234–3244.

[23] F.M. Green, A.G. Shard, I.S. Gilmore, M.P. Seah, Analysis of the interface and its position in $C_{60}{}^{n+}$ secondary ion mass spectrometry depth profiling, Anal. Chem. 81 (2008) 75–79.

[24] V. Cristaudo, S. Collette, N. Tuccitto, C. Poleunis, L.C. Melchiorre, A. Licciardello, F. Reniers, A. Delcorte, Molecular surface analysis and depth-profiling of polyethylene modified by an atmospheric Ar-$D_2O$ post-discharge, Plasma Processes Polym. 13 (2016) 106–1119.

[25] V. Cristaudo, C. Poleunis, B. Czerwinski, A. Delcorte, Ar cluster sputtering of polymers: effects of cluster size and molecular weights, Surf. Interface Anal. 46 (2014) 79–82.

[26] M.J. Genet, C.C. Dupont-Gillain, P.G. Rouxhet, XPS analysis of biosystems and biomaterials, Med. Appl. Colloids (2008) 177–307.

[27] S. Kayser, D. Rading, R. Moellers, F. Kollmer, E. Niehuis, Surface spectrometry using large argon clusters, Surf. Interface Anal. 45 (2013) 131–133.

[28] J.C. Vickerman, D. Briggs, TOF-SIMS - Surface Analysis by Mass Spectrometry, IMPublications, Chichester, UK, 2001, p. 753.

[29] A. Delcorte, Matrix-enhanced secondary ion mass spectrometry: The Alchemist's solution? Appl. Surf. Sci. 252 (2006) 6582–6587.

[30] J. Cheng, A. Wucher, N. Winograd, Molecular depth profiling with cluster ion beams, J. Phys. Chem. B 110 (2006) 8329–8336.

[31] I.S. Gilmore, M.P. Seah, Investigating the difficulty of eliminating flood gun damage in TOF-SIMS, Appl. Surf. Sci. 203 (2003) 600–604.

[32] R. Havelund, M.P. Seah, A.G. Shard, I.S. Gilmore, Electron flood gun damage effects in 3D secondary ion mass spectrometry imaging of organics, J. Am. Soc. Mass Spectrom. 25 (2014) 1565–1571.

[33] A.G. Shard, R. Havelund, M.P. Seah, S.J. Spencer, I.S. Gilmore, N. Winograd, D. Mao, T. Miyayama, E. Niehuis, D. Rading, R. Moellers, Argon cluster ion beams for organic depth profiling: results from a VAMAS interlaboratory study, Anal. Chem. 84 (2012) 7865–7873.

[34] A. Delcorte, K. Moshkunov, M. Debongnie, Relationships between crater and sputtered material characteristics in large gas cluster sputtering of polymers: results from molecular dynamics simulations, J. Vac. Sci. Technol., B 36 (2018) 03F109.

[35] S. Surana, T. Conard, C. Fleischmann, J.G. Tait, J.P. Bastos, E. Voroshazi, R. Havelund, M. Turbiez, P. Louette, A. Felten, C. Poleunis, Understanding physico-chemical aspects in the depth profiling of polymer: fullerene layers, J. Phys. Chem. C 120 (2016) 28074–28082.

[36] M.P. Seah, S.J. Spencer, Ultrathin $SiO_2$ on Si II. Issues in quantification of the oxide thickness, Surf. Interf. Anal.: Int. J. Devoted Develop. Appl. Techn. Anal. Surf., Interfaces Thin Films 33 (2002) 640–652.

[37] M.P. Seah, S.J. Spencer, Attenuation lengths in organic materials, Surf. Interface Anal. 43 (2011) 744–751.

[38] R. Havelund, M.P. Seah, I.S. Gilmore, Sampling depths, depth shifts, and depth resolutions for $Bi_n{}^+$ ion analysis in argon gas cluster depth profiles, J. Phys. Chem. B 120 (2016) 2604–2611.

[39] A. Delcorte, C. Leblanc, C. Poleunis, K. Hamraoui, Computer simulations of the sputtering of metallic, organic, and metal-organic surfaces with $Bi_n$ and $C_{60}$ projectiles, J. Phys. Chem. C 117 (2013) 2740–2752.

[40] A. Delcorte, V. Cristaudo, V. Lebec, B. Czerwinski, Sputtering of polymers by keV clusters: microscopic views of the molecular dynamics, Int. J. Mass Spectrom. 370 (2014) 29–38.

[41] C. Poleunis, V. Cristaudo, A. Delcorte, Temperature dependence of $Ar_n{}^+$ cluster backscattering from polymer surfaces: a new method to determine the surface glass transition temperature, J. Am. Soc. Mass Spectr. 29 (2018) 4–7.

[42] M.P. Seah, Universal equation for argon gas cluster sputtering yields, J. Phys. Chem. C 117 (2013) 12622–12632.

[43] A. Delcorte, M. Debongnie, Macromolecular sample sputtering by large Ar and CH$_4$ clusters: elucidating chain size and projectile effects with molecular dynamics, J. Phys. Chem. C 119 (2015) 25868–25879.

[44] D. Kuck, Mass spectrometry of alkylbenzenes and related compounds. Part I. Gas-phase ion chemistry of alkylbenzene radical cations, Mass Spectrom. Rev. 9 (1990) 187–233.

[45] A. Delcorte, P. Bertrand, Energy distributions of hydrocarbon secondary ions from thin organic films under keV ion bombardment: correlation between kinetic and formation energy of ions sputtered from tricosenoic acid, Nucl. Instrum. Methods Phys. Res. Sect. B: Beam Interact. Mater. Atoms 117 (1996) 235–242.

[46] A. Delcorte, P. Bertrand, Influence of chemical structure and beam degradation on the kinetic energy of molecular secondary ions in keV ion sputtering of polymers, Nucl. Instrum. Methods Phys. Res., Sect. B 135 (1998) 430–435.

[47] L. Rzeznik, B. Czerwinski, B.J. Garrison, N. Winograd, Z. Postawa, Microscopic insight into the sputtering of thin polystyrene films on Ag 111 induced by large and slow Ar clusters, J. Phys. Chem. C 112 (2008) 521–531.

[48] L. Rzeznik, R. Paruch, B. Czerwinski, B.J. Garrison, Z. Postawa, Sputtering of thin films of bariated molecules of arachidic acid by large noble gas clusters, Vacuum 83 (2009) S155–S158.

[49] T. Kawashima, T. Kurosawa, S. Aoyagi, S. Sheraz, J.S. Fletcher, M. Futigami, N.P. Lockyer, J.C. Vickerman, Examination of fragment ions of polystyrene in TOF-SIMS spectra using MS/MS, Surf. Interface Anal. 46 (2014) 92–95.

[50] R. Möllers, N. Tuccitto, V. Torrisi, E. Niehuis, A. Licciardello, Chemical effects in C$_{60}$ irradiation of polymers, Appl. Surf. Sci. 252 (2006) 6509–6512.

[51] T. Aoki, Molecular dynamics simulations of cluster impacts on solid targets: implantation, surface modification, and sputtering, J. Comput. Electron. 13 (2014) 108–121.